Inferior temporal cortex leads prefrontal cortex in response to a violation of a learned sequence.

Hamideh Esmailpour[1,2], Rajani Raman[1,2] and Rufin Vogels[1,2]

[1]Laboratorium voor Neuro- en Psychofysiologie, Department of Neurosciences, KU Leuven

[2]Leuven Brain Institute, KU Leuven, Belgium

Corresponding author: rufin.vogels@kuleuven.be

Keywords: statistical learning, predictive coding, inferior temporal cortex, prefrontal cortex, expectation suppression

Abstract

Primates learn statistical regularities that are embedded in visual sequences, a form of statistical learning. Single-unit recordings in macaques showed that inferior temporal (IT) neurons are sensitive to statistical regularities in visual sequences. Here we asked whether ventrolateral prefrontal cortex (VLPFC), which is connected to IT, is also sensitive to transition probabilities in visual sequences and whether the statistical learning signal in IT originates in VLPFC. We recorded simultaneously multi-unit activity (MUA) and local field potentials (LFPs) in IT and VLPFC after monkeys were exposed to triplets of images with a fixed presentation order. In both areas, the MUA was stronger to images that violated the learned sequence (deviants) compared to the same images presented in the learned triplets. The high-gamma and beta LFP power showed an enhanced and suppressed response, respectively, to the deviants in both areas. The enhanced response was present also for the image following the deviant, suggesting a sensitivity for temporal adjacent dependencies in IT and VLPFC. The increased response to the deviant occurred later in VLPFC than in IT, suggesting that the deviant response in IT was not inherited from VLPFC. These data support predictive coding theories that propose a feedforward flow of prediction errors.

Keywords: statistical learning, predictive coding, inferior temporal cortex, prefrontal cortex, expectation suppression.

Introduction

Animals and humans learn temporal regularities in their environment (for reviews, see Krogh et al. 2012; Turk-Browne 2012; Dehaene et al. 2015), which is a form of statistical learning. The learning of transition probabilities of successively presented visual images changes the response of macaque inferior temporal (IT) neurons and fMRI activations in the human occipito-temporal cortex. Indeed, exposure to a set of fixed sequences of visual images produces a smaller IT response to an image in its learned sequence compared to the response to the same image when positioned in one of the other sequences (Meyer and Olson 2011; Meyer et al. 2014; Ramachandran et al. 2016; Kumar et al. 2017; Ramachandran et al. 2017; Schwiedrzik and Freiwald 2017; Kaposvari et al. 2018). An enhanced activation to stimuli that violated the learned sequences, "deviants", has also been found in the human occipito-temporal cortex (Richter et al. 2018; Richter and de Lange 2019), using a similar paradigm as in most of the macaque studies. These studies demonstrated that ventral stream neurons are sensitive to the order of the stimuli presented in a sequence (Meyer and Olson 2011; Kaposvari *et al.* 2018), which differs from the order-invariant encoding of stimulus associations (Sakai and Miyashita 1991; Li and Dicarlo 2008).

The difference in response between the deviant and the stimulus at its correct position in the learned sequence can result from two, not mutually exclusive, mechanisms. First, it can result from "expectation suppression", which is the reduced response to a stimulus at its predicted position in the sequence compared to the deviant. Alternatively, it can reflect "surprise enhancement", which corresponds to an increase of the response to the deviant stimulus. Both mechanisms can be dissociated by having a neutral condition, e.g. sequences of randomly ordered stimuli, as reference (Ramachandran *et al.* 2017; Kaposvari *et al.* 2018;

Feuerriegel et al. 2021). Two studies that examined these mechanisms in macaque IT provided evidence for both (Ramachandran *et al.* 2017; Kaposvari *et al.* 2018) but differed in the degree to which each of these two factors contributed most to the difference in response between the deviant and the original stimulus sequence. Furthermore, a human MEG study found no evidence for expectation suppression but observed surprise enhancement for sequences of visual images, with estimated sources in the occipito-temporal cortex (Manahova et al. 2018). Because of the discrepant results between the previous studies and since we did not employ a neutral condition in the present experiment, we will employ here "deviant response" as a descriptive label for the difference in response between the deviant and the correctly positioned stimulus in a sequence, but this without implying that it reflects surprise enhancement instead of expectation suppression.

Previous single- and multi-unit recording studies of visual statistical learning focused on IT. However, IT is not an isolated area but a part of several networks of interconnected areas (Kravitz et al. 2013). Other brain regions, connected with IT, might also show deviant responses following statistical learning. It is unclear how potential deviant responses in the areas connected to IT relate and/or contribute to those observed in IT. Here, we examined deviant responses in the caudal ventrolateral prefrontal cortex (VLPFC). The choice of this area as a recording target was based on multiple reasons. First, monkey fMRI studies in our laboratory (Vergnieux and Vogels 2020) showed that VLPFC is one of few areas outside the ventral visual stream that are activated by visual image sequences during passive fixation following the long exposure to image sequences during statistical learning**,** as employed in previous IT studies. An area that is activated by a visual stimulus is a candidate to learn temporal regularities of the visual sequences. Second, VLPFC is connected with IT (Webster et al. 1994; Bullier et al. 1996; Markov et al. 2014; Saleem et al. 2014; Giarrocco and Averbeck

2021; Xu et al. 2021). Third, VLPFC neurons, particularly caudally, can have shorter response latencies than IT neurons (Verhoef et al. 2008; Riley et al. 2017; Caprara et al. 2018), and thus can contribute to the onset of deviant responses in IT. The early onset of the caudal VLPFC neurons suggests that their visual input may come from dorsal stream areas, which show image-selective response with a latency earlier than IT neurons (Sereno and Maunsell 1998; Srivastava et al. 2009). Indeed, this part of VLPFC also receives input from the intraparietal sulcus (Bullier *et al.* 1996; Xu *et al.* 2021). Fourth, statistical learning of auditory sequences generated with an artificial grammar activates macaque caudal VLPFC area 45 (Wilson et al. 2015). Furthermore, field potential recordings have implicated prefrontal cortex in predictive processing of brief auditory sequences (Chao et al. 2018), although it is unclear whether this involves working memory instead of long-term memory of stimulus sequences. Also, studies employing auditory oddball paradigms suggested a contribution of the prefrontal cortex to signals of the mismatch between predicted and presented stimuli in macaques (Camalier et al. 2019) and humans (Durschmid et al. 2016; Nourski et al. 2018). Note however that similar visual oddball paradigms do not produce a deviant response in macaque IT (Kaliukhovich and Vogels 2014).

Human fMRI studies of visual statistical learning using a similar paradigm as that employed in most single unit IT studies disagree about the presence of visual deviant responses in the prefrontal cortex. One study found no evidence of prefrontal cortical activation to deviant sequences after statistical learning (Richter *et al.* 2018) but another study observed activations when the stimuli were task-relevant (Richter and de Lange 2019), suggesting that the occurrence of deviant response in the prefrontal cortex depends on the task relevancy of the stimuli. Human fMRI studies employing other statistical learning paradigms showed less activation for predicted compared to unpredicted stimuli in the prefrontal cortex (Aizenstein

et al. 2004; Rosenthal et al. 2016; Rosenthal et al. 2018). Given the discrepancies amongst the human fMRI studies, it was an open question whether we would observe visual deviant responses in macaque VLPFC during passive fixation.

In the present study, we assessed whether the VLPFC shows a deviant response after the monkeys learned the statistical regularities of 5 sequences that consisted of 3 images (triplets) each, following the paradigm of (Meyer *et al.* 2014). We also compared the properties of the deviant response with those in IT using simultaneous recordings from both areas. One property relates to what these areas learn about the stimulus sequence. Previous studies indicate that IT neurons learn predominantly adjacent stimulus dependencies (Meyer *et al.* 2014; Kaposvari *et al.* 2018), i.e. pairwise, serial transitions of immediately succeeding stimuli. Prefrontal neurons may integrate information across longer intervals (Wolff et al. 2022) and thus may encode non-adjacent stimulus dependencies. In the present study, we replaced only the second stimulus of a triplet with a stimulus of another triplet. Learning of only adjacent dependencies would produce a stronger response not only for the second stimulus, i.e. the deviant, but also for the third stimulus of the triplet. Indeed, the third stimulus will deviate from the stimulus predicted by the preceding deviant stimulus. This response pattern was found previously for IT neurons (Meyer *et al.* 2014; Kaposvari *et al.* 2018). A smaller or no enhanced response to the third stimulus, being predicted by the first stimulus but not by the second deviant, would suggest learning of non-adjacent dependencies.

A second property relates to the timing of the deviant response in the two areas. The deviant response in IT may originate in the prefrontal cortex. The prefrontal cortex would detect a mismatch between the deviant and the learned, expected stimulus, and this “surprise signal” would then enhance the response of IT neurons. This hypothesis is in line with the top-down

flow of prediction error signals as postulated in the theory of cortical function by Heeger (Heeger 2017). If this is true, then one would predict a faster onset of the deviant response in VLPFC compared to the IT cortex. On the other hand, predictive coding theories which propose a feedforward flow of prediction errors (Friston 2005) predict an earlier deviant response in IT than in VLPFC.

We exposed two monkeys to five triplets of images of animals. The VLPFC region we recorded from was defined based on earlier fMRI mapping data obtained in the same monkeys and thus was known to respond to visual images of animals presented during passive fixation. The IT region we recorded from was the ventral bank of the middle Superior Temporal Sulcus (STS) since electrical microstimulation of the VLPFC region showed fMRI activation in that STS region in one of our monkey subjects, suggesting connectivity between the mid-STS and VLPFC. Because we do not know how long the exposure to visual sequences needs to be to obtain deviant responses in IT and VLPFC, we exposed the monkeys to the triplets in daily sessions for several weeks, as was done in previous IT recording studies on statistical learning. After the exposure, we measured multi-unit activity (MUA) and local field potentials in IT and VLPFC simultaneously, comparing responses to the same stimuli when these were presented in the learned triplets and in triplets in which the second stimulus was a deviant.

Materials and Methods

Subjects and surgery.

Two female rhesus monkeys, M1 (7 kg; age: 11 years) and M2 (5 kg; age: 14 years) participated in this study. They were implanted with an MRI-compatible headpost for fixing the head during the experiments, using standard procedures under full anesthesia and aseptic conditions.

In addition, two MRI-compatible recording chambers, targeting VLPFC and the mid-STS of one hemisphere were secured to their skull with ceramic screws and dental cement. Animal care and experimental procedures complied with the regional (Flanders), European, and National Institute of Health guidelines and were approved by the Animal Ethical Committee of KU Leuven.

Recording locations.

The targeted regions in VLPFC and IT (Figure 1) were defined based on earlier fMRI mapping experiments in each animal and a combined fMRI-electrical microstimulation study in M1. Before the fMRI mapping experiments, complex images (different from the ones employed in the present study) were presented for several weeks in sequences (quartets (Vergnieux and Vogels 2020) or doublets) during passive fixation. Subsequent scanning during passive fixation showed activations to the image sequences, relative to a fixation target-only condition, in ventral visual stream areas and VLPFC. The VLPFC activation was in the ventral bank of the caudal part of the principal sulcus and the anterior bank of the inferior ramus of the arcuate sulcus (area 45). These prefrontal fMRI activations to sequences of highly familiar images were similar to those obtained previously when contrasting images of objects with their mosaic scrambled versions (Denys et al. 2004). In M1, we stimulated electrically the activated area (300 μA at 300 Hz) while the animal was fixating a small target in the MRI scanner (Ekstrom et al. 2008). Electrical microstimulation of this VLPFC region produced activations, relative to interleaved no-electrical stimulation blocks, in the ventral bank of the mid-STS, which guided the location of the IT recordings in the present study.

To record from the VLPFC target without damaging it with a guide tube, we implanted the recording chamber under an oblique angle in the coronal plane. The IT chamber was implanted under an angle in the sagittal plane, approaching the mid-STS posteriorly. This design allowed implantation of both recording chambers on the same hemisphere and placement of microdrives for simultaneous recordings from the two areas.

Recordings.

We performed simultaneous recordings from IT and VLPFC with two 8 channel V-probes (Plexon) with 150um electrode spacing. Each probe was lowered with a Narishige microdrive (MO-97A) through a guide tube that was positioned in a Crist grid which was fixed into the recording chamber. The grid positions and recording depths were based on structural MRI scans in which we visualized the recording chamber, grid, and capillaries inserted into grid holes. The capillaries were filled with a copper sulfate solution. The recording chamber and the grid were made visible by filling the chamber with a saline solution of the contrast agent Gadolinium. The actual recording depths of the electrodes in each penetration depended on the gray-white matter transitions and of the silence associated with a sulcus that were observed while lowering the probes into the brain.

The stainless steel guide tube was grounded and the grounded stainless steel needle of the V-probe served as a reference. We used a Plexon data acquisition system (Plexon Inc.) for amplification and filtering of the electrical signals. Recorded signals were preamplified with a headstage having an input impedance of >1GΩ. The signals were bandpass filtered between

250 to 8000 Hz for on-line recordings of spikes. Unfiltered broadband signals were recorded simultaneously with a sampling rate of 40 kHz.

Eye position and pupil diameter were measured online with an infrared-based eye-tracking system (ISCAN EC-240A, ISCAN Inc.; 120 Hz sampling rate). The eye positions and pupil size was saved with a sampling frequency of 1 kHz. We employed fixation windows that measured 2° on a side. The horizontal and vertical eye position, pupil diameter, stimulus-related and behavioral events were recorded simultaneously with spiking and broadband neural activity and stored for later off-line analysis on a computer that was synchronized with the Plexon data acquisition system.

After lowering the V Probes, we checked in each area whether channels showed spiking activity and were visually responsive. We waited for at least one hour after probe insertion to obtain stable recordings. We recorded from 5 and 2 grid positions of the IT chamber in monkey M1 and M2, respectively, and from 2 grid positions of the prefrontal chamber in each monkey. In both areas, the recorded depths differed among the daily penetrations. The analyzed data were obtained from 28 and 24 successful penetrations in M1 and M2, respectively.

Stimuli.

The stimulus consisted of 30 color images of animals. Each image fitted into a 4° wide square. The mean luminance of each RGB channel was equated across images using the Shine toolbox (Willenbockel et al. 2010). The images had a gray background. The gamma-corrected stimuli were presented on a CRT monitor (Phillips Brilliance 202P4, frame rate = 75 Hz, resolution = 1024 × 768 pixels) located approximately 58 cm from the subject's eyes. The images were presented at the center of the display. Together with the first frame of each

image, we presented a small white square, invisible to the monkey, at the bottom left corner of the monitor. A photodiode measured the onset of the square and that signal was sampled by a computer at 40 kHz.

The 30 images were divided into two sets of 15 images each. For each monkey, the 15 images of one set were grouped in 5 triplets. One of the two sets served as stimuli for the triplets for one monkey (see Figure 2A for one set), while the other set was used to make the triplets for the other monkey. The order of the images within a triplet was fixed ("fixed sequence"). The 15 images of the remaining set of each monkey were presented in a pseudorandom order ("random sequence") during the exposure phase and some recording sessions. The fixed and random sequences were presented in different blocks.

Task.

The monkeys were performing a fixation task during stimulus presentation for a juice reward (Figure 2C). A trial started with the onset of a small, 0.13° wide red square which served as a fixation target. Then, three images were shown in succession for 506 ms each back to back, i.e. without interstimulus interval. After the offset of the third image, the fixation target remained on the screen for a variable period, ranging from 300 to 500 ms, followed by the delivery of a juice reward. The reward was given only when the monkey fixated during the whole trial. Failure of fixation within the trial period halted the stimulus presentation.

Exposure phase.

During the exposure phase, both monkeys were shown the fixed and random sequences in blocks of 125 trials while performing the passive fixation task. In the case of a fixed sequence

block, each of the 5 triplets was presented 25 times in random order. We will not describe the random blocks here since these were not analyzed for the present study (data were obtained only for M1). Random and fixed sequences blocks alternated in a daily session.

We exposed the monkeys to the triplets for several weeks (M1: 21 days; M2: 23 days). The total number of unaborted trials per triplet was 2250 and 1825 for M1 and M2, respectively, before the recordings started.

Recording phase.

In both monkeys, the initial recordings were done using both fixed and random sequences blocks, but the random sequences were presented only in a couple of sessions in M2. Since this monkey did not perform that well, we decided to prioritize data collection for the fixed sequences. We will describe below only the recordings for the fixed sequence blocks.

During the recording phase, the fixed sequence blocks consisted of two types of trials. The first type of trial consisted of one of the five triplets of the fixed sequences, identical to those of the exposure phase. We will label these as fixed triplets (Figure 2B). The second type of trial included a deviant: the second stimulus (S2) of a triplet was replaced by the second stimulus of one of the other four triplets (Figure 2B). The first (S1) and third stimulus (S3) of a deviant triplet were identical to that of the corresponding fixed triplet. Since there were 5 fixed triplets, we had in total 20 deviant triplets. Each of the 20 deviant triplets was presented once in a block of 125 trials, while the remaining 105 trials were fixed triplets, each of the 5 fixed triplets being presented with the same frequency (21). In our design, the same image occurred with an equal relative frequency (0.2) in a fixed and deviant triplet. Note that the triplet of an aborted trial was presented again later in the same block. Only unaborted trials were analyzed

further. We kept the proportion of deviant trials per block (16%) rather low to avoid the extinction of the learned stimulus transitions in the fixed triplets.

Data analysis.

MUA

The broadband signal was filtered with a high-pass filter (8 pole Butterworth; cut-off frequency = 400 Hz), using Plexon Offline Sorter. Trials in which the signal was clipped were removed from further analysis. Offline sorting of spikes was performed with Offline Sorter (Plexon) using a threshold set above the noise band. All spikes that crossed the threshold recorded by one channel defined one MUA unit. Thus, no attempt was made to isolate single units. The spike sorting was done for all the data of a block simultaneously and was performed blindly about which triplet was presented.

We included for further analysis only blocks of units that showed a significant modulation of the MUA during a trial. This was tested for each unit, as follows. We divided the trial into eight 253 ms long analysis windows, starting 253 ms before the onset of S1, and computed the spike count for each window per trial. For each block, we ran two repeated measures ANOVAs, one including the fixed triplet trials and a second one that contained only the deviant triplet trials. A block of a unit was retained when either one of the ANOVAs showed a significant effect ($p < 0.025$) of the factor analysis window on the response, i.e. its MUA was modulated significantly during the trial. These tests treated each of the three stimuli of a triplet equally, without biasing the selection for units responding to S1 (unlike (Meyer *et al.* 2014).

We computed the mean spike firing rate across all the significant blocks for an MUA unit and this separately for the fixed and deviant triplets. Thus, each daily session contributed maximally 8 MUA units per area. This procedure resulted in 148 and 168 units for IT in M1 and M2, respectively, and 164 and 179 units for VLPFC in M1 and M2, respectively. We computed population peristimulus time histograms (PSTH) by averaging the firing rates across units, after subtracting the baseline activity per unit. 95% confidence intervals of the mean firing rate for each bin were computed by bootstrapping units (Matlab function "bootci"; Bias corrected and accelerated percentile method). We computed the difference between the mean firing rate for the deviant and fixed triplets in bins of 11 ms for each unit. 95% confidence intervals of the mean difference for each bin were obtained by bootstrapping of units.

To assess whether the mean response differed between deviant and fixed triplets, we computed for each unit the mean net firing rate for the three stimuli of a triplet, using three 506 ms analysis windows that started 50ms after the onset of S1, S2, and S3, respectively. Then, we performed a two-way, repeated-measures ANOVA with factors stimulus order and deviant versus fixed triplets. The difference in mean response between deviant and fixed triplets was tested for S1, S2, and S3 separately with Wilcoxon signed-rank tests, corrected for multiple comparisons ($p < 0.017$). All these analyses were performed on the data of each monkey separately.

We employed bootstrapping to compute the confidence interval of the difference in latency of the deviant response between IT and VLPFC. We resampled with replacement the units of our recorded IT sample and of the VLPFC sample, thus obtaining new IT and VLPFC samples. For each of the new pairs of (resampled) samples, which had the same size as the original samples, we computed the latency difference. The latency was quantified as the first 11 ms

bin of 4 successive bins for which the mean difference in firing rate to S2 between the deviant and fixed triplets was greater than twice the standard deviation of the differences in mean response for the bins ranging between -253 ms and 506 ms relative to S1 onset. We took the S1 responses also into account to compute the standard deviation of the baseline differences since no difference in response between deviant and fixed triplets is expected (and was not present) for S1 (the deviant stimulus was S2). The estimated latency for the VLPFC units was subtracted from the latency of the deviant response of the IT units. The resampling of the units was performed 1000 times, resulting in 1000 latency differences. Percentile 2.5 and 97.5 of the distribution of the 1000 latency differences defined the 95% confidence interval of the difference in response latency.

To assess the significance of the difference between the latency of the S2 deviant response in our samples of IT and VLPFC neurons, we employed a permutation test. We concatenated the units of the two areas and shuffled the area labels and then derived the latency for the newly created surrogate IT and VLPFC samples. The two surrogate samples had the same number of neurons, but now with different labels, as the original IT and VLPFC samples. We employed the same latency estimation method as we used for the computation of the confidence interval of the latency difference (see above). We permuted the data 1000 times, obtaining 1000 latency differences under the null hypothesis of no difference in latency of the deviant response between the two areas. The p-value corresponded to the percentile of the originally observed latency difference or was set to $p < 0.001$ when the observed latency difference was outside the null distribution. This test was performed for the data of each monkey separately and the data pooled across monkeys.

LFP power

We downsampled the broadband signal to 1000 Hz and applied a digital notch filter (fourth-order Butterworth FIR filter; Fieldtrip Toolbox, F.C. Donders Centre for Cognitive Neuroimaging, Nijmegen, The Netherlands) for 50 Hz (AC line noise) and 75 Hz (the display's frame rate). We removed outlier trials in which the signal was <1% or >99% of the total input range, which also protected against clipping. By convolving single-trial data using complex Morlet wavelets and taking the square of the convolution between the wavelet and signal, the time-varying power of the signal for a frequency was obtained. As in previous studies (e.g. (De Baene and Vogels 2010; Kaliukhovich and Vogels 2011; Popivanov et al. 2014), the Morlet wavelets had a constant center frequency-spectral bandwidth ratio f0/σf of 7, with f0 ranging from 1 to 150 Hz in steps of 1 Hz. We removed outlier trials that showed an extraordinarily high power (maximum baseline-normalized power during triplet presentation > 500; baseline: 0- 200 ms before S1 onset).

For each block and channel combination, we randomly selected the same number of fixed triplet trials that had the same S2 images as in the deviant triplets. Thus, S2 images of the deviant and fixed triplets were identical. Also, this procedure equated the number of fixed and deviant triplets for each block and channel combination. Then, we averaged for each daily session the spectral power across all the blocks per channel. Next, we computed the mean spectral power across channels per day, using a weighted average that considered the number of selected trials for the different channels. This was done separately for the deviant and fixed triplets. Thus, we obtained one mean time-frequency power matrix per daily session for each area. These were then averaged across days. The normalized power was expressed for each frequency in dB: 10*log10 (power(f,t)/ baseline power(f)), with power (f,t) being the spectral power for frequency f at time t and baseline power(f) the mean spectral power for frequency f in a 200 ms window that started 200 ms before S1 onset.

To assess the statistical significance of the difference in power between deviant and fixed triplets in the time-frequency domain, we employed a randomization test in which we randomized the sign of the difference of the power between the two conditions per daily session (1000 randomizations), thus creating a null distribution of mean differences in power across sessions. The mean difference in power was transformed to a z-score using the mean and standard deviation of this null distribution. The z-scores were thresholded at $p = 0.025$ (two-sided; standard normal distribution) and then corrected for multiple comparisons using the cluster-based method (the cluster statistic was the number of time-frequency points of a thresholded cluster; 1000 permutations; see (Cohen 2014). The multiple comparison correction was applied for the period from S1 onset till 200 ms after S3 offset.

For further statistical analyses, we averaged for each area and daily session the spectral power, computed as described above, in two frequency bands: a high-gamma band ranging from 51 to 80 Hz and a beta band ranging from 12 to 30 Hz. The spectral power in these bands was averaged within each of three 506 ms windows that started 50 ms after S1, S2, and S3 onset, respectively. Then, we performed a two-way, repeated-measures ANOVA with factors stimulus order and deviant versus fixed triplets, followed by Wilcoxon signed-rank tests. The analyses were performed on the data of each monkey separately. 95% confidence intervals of the mean power were computed by bootstrapping daily sessions.

Granger causality analysis.

Since we recorded simultaneously from IT and VLPFC, we employed Granger causality (GC) analysis of the LFPs to estimate directional information flow between the areas during the presentation of the triplets. We selected for each daily session the channel pairs that showed a significant modulation of the spiking activity by the images (ANOVA; see above), ensuring

that the selected channel was inside the cortical gray matter. First, we filtered the LFP signals using a 3rd order Butterworth high-pass filter with a cutoff frequency of 3Hz (Seth 2010), followed by downsampling of the signal to 250 Hz (Pagnotta et al. 2018). Then, for each channel and day, we concatenated the artifact-free trials (see above) and z-scored the concatenated LFPs across time per day for each channel. This was followed by a z-scoring per time-point across trials for each daily session to reduce non-stationarity (Ding et al. 2000). The z-scoring was done for the deviant and fixed triplets separately. We used the FieldTrip toolbox (Oostenveld et al. 2011) to compute non-parametric GC (Dhamala et al. 2008). Note that non-parametric GC does not require determination of the model order of the autoregressive model as is needed in parametric GC. The spectral power was computed with multitaper spectral analysis, using 5 tapers and a window of 250 ms in steps of 50 ms. The GC was computed for both directions (IT to VLPFC and VLPFC to IT) for all selected channel pairs and then averaged across the pairs per daily session. The average GC across days was then plotted as a function of time and frequency. For statistical analyses, we computed the mean GC for each direction for two frequency bands: 20-40 Hz and 51-80 Hz. The latter is the same high-gamma band that we employed to analyze the LFP power (see above), while the former band was defined based on inspection of the GC values in the time-frequency plots. We assessed whether the mean GC values in each of the two frequency bands were higher than expected by chance by computing null distributions of the mean GC in each of the frequency bands after shuffling the order of trials for a channel of each pair. The permutation of trials was performed 100 times, and the 95th percentile of the null distribution was taken as the threshold for significance. All original mean GC values for the high-gamma and low-frequency bands were well above this threshold. To visualize the timecourse of the GC values per band and direction, we first z-scored the GC values averaged across channel pairs per day and computed the mean z-scored

GC values. Confidence intervals were computed by bootstrapping the z-scored mean GC values of daily sessions.

The dominant direction of information flow was computed by subtracting the GC for IT to VLPFC from the GC for VLPFC to IT in each frequency band. The estimated direction of information flow using GC analysis can be affected by differences in power and signal-to-noise ratio between the areas (Bastos and Schoffelen 2015). To assess this, we employed time-reversed GC (TRGC), analysis. TRGC also can protect against common reference issues (Pagnotta *et al.* 2018). We found that the dominant GC direction reversed when time-reversing the signal for the low-frequency band in both monkeys – as expected when it is not due to differences in power or signal-to-noise ratio (Bastos and Schoffelen 2015) - but not for the high-gamma band in one monkey. Thus, we will report only the GC values for the low-frequency band. For this band, the confidence intervals of the differences in GC were computed by bootstrapping differences in z-scored GC values of the daily sessions. The z-scoring was performed for each daily session using the mean GC values, averaged across channel pairs. For this analysis of the difference in GC scores between directions, we concatenated for each daily session the data of the two directions and performed the z-scoring on the concatenated data; otherwise, the difference in GC between the two directions would have been abolished.

Pupil size

For each trial, we smoothed the pupil size data with a 200 ms Hamming window. We equated the number of deviant and fixed triplet trials by randomly selecting 4 trials for each of the 5 fixed triplets per block. Then, we averaged the pupil diameter data for the 20 deviant and the

20 pseudorandomly selected fixed triplet trials that had the same S2 images as in the deviant triplets, followed by subtraction of the mean "baseline" pupil size averaged in a 506 ms window that started 506 ms before S1 onset. Then, we z-scored the baseline-subtracted mean pupil sizes after concatenating the fixed and deviant triplet conditions. Thus, we obtained for each block z-scored pupil size measures for the fixed and deviant triplets. These were averaged per subject and 95% confidence intervals were computed by bootstrapping blocks.

To assess the statistical difference of a difference in pupil size between the two types of triplets for each monkey, we averaged for each block the z-scored pupil sizes in three 506 ms windows that started 300ms after the onset of S1, S2, and S3, respectively. The 300 ms delay was employed because of the relatively long latency in pupil size responses, compared to cortical neural responses, in cognitive tasks in macaques (Ebitz et al. 2014; Pagliaccio et al. 2019; Peter et al. 2021). For statistical testing, we performed a repeated-measures ANOVA with within-block factors stimulus order and deviant versus fixed triplet. This was followed by Wilcoxon signed-rank tests for each stimulus order. Based on earlier studies of pupil size changes in monkeys, we took a conservative onset of the analysis window, i.e. 300 ms. Note that the pupil responses last relatively long and using such a conservative window onset should not have affected capturing the main effect. We verified this empirically by using two additional 506 msec long windows that started at 200 and 250 ms, respectively. For these earlier windows, Wilcoxon signed-rank tests on the pupil size data, analyzed following the same procedure as for the 300 ms onset window, showed qualitatively identical significant effects in each monkey.

Results

We exposed two monkeys to 5 triplets of visual images while they were performing a passive fixation task. During the exposure, the order of the 3 images was fixed ("fixed triplets"). After this exposure phase, we presented the monkeys with the same fixed triplets, interleaved with less frequent presentations of triplets in which the second image (S2) was taken from one of the other triplets ("deviant triplets"; Figure 2B). We recorded simultaneously from IT and VLPFC multi-unit activity (MUA) and LFPs during this test and compared the responses to the fixed and deviant triplets for each area. Before presenting the electrophysiological data, we will provide behavioral evidence, based on analyses of pupil size, that the monkeys learned the regularities that were embedded in the sequences.

Pupil size

We measured the pupil size while the monkey was fixating the fixation target before, during, and after the presentation of the triplets in the MUA/LFP recording sessions. The triplets were presented in blocks of 125 trials, of which 20 contained deviant triplets and the remaining ones were fixed triplets. For each block, we compared the average pupil size for the 20 deviant triplets and 20 pseudorandomly selected fixed triplets, making sure that the same S2 images were presented with the same frequency in the two kinds of selected triplets. The mean z-scored pupil size averaged across blocks, was smaller for the deviant compared to the fixed triplets for each monkey (Figure 3). For quantitative statistical analysis, we averaged per block the mean pupil size in three windows of 506ms, which started 300 ms after image onset (S1, S2, and S3; see Methods). Because the deviant occurred for S2 but not S1, we expected to see no difference in pupil size between the two triplet conditions for S1, resulting in an interaction of the stimulus order (S1, S2, and S3) and the triplet conditions. A repeated-measures ANOVA indeed showed a significant interaction of these factors in each monkey (M1: $F(1.7, 218.3) =$

98.2, p = 3.68 * 10^{-28}, N = 128 blocks; M2: F(1.7, 197.6) = 4.45, p = 0.018, N = 118; Greenhouse-Geiser correction). Wilcoxon signed-rank tests showed a significant difference in pupil size between the fixed and deviant triplets for S2 in each monkey (M1: p =0.000002; M2: p = 0.008), while this difference reached significance (Bonferroni-adjusted alpha value = 0.017) in one monkey for S3 (M1: p = 0.000006; M2: p = 0.16). As expected because the deviant can occur only after S1, there was no significant difference between the pupil sizes for the deviant and fixed triplets for S1 (M1: p = 0.40; M2: p = 0.47). Since the triplets differed only in transition probabilities (images were identical in the two sorts of triplets), these pupil size data provide behavioral evidence of sequence learning in each monkey.

MUA

We recorded MUA simultaneously in IT and VLPFC in two monkeys. The recording sites in IT were in the ventral bank of the middle of the STS (Figure 1), while those in VLPFC were ventral to the posterior part of the principal sulcus, encroaching the anterior bank of the inferior ramus of the arcuate sulcus (Figure 1). In each area, we lowered the laminar probe to a depth at which visual responses were present, based on earlier recordings.

In agreement with previous studies (Meyer and Olson 2011; Meyer *et al.* 2014; Kaposvari *et al.* 2018), the mean MUA in IT was significantly larger for the deviant S2 compared to the same S2 images presented in fixed triplets (Wilcoxon signed-rank test; M1: p = 0.000001; N = 148 units; M2: p = 6.18 * 10^{-28}; N = 168; Figure 4A & C). As observed previously (Meyer *et al.* 2014; Kaposvari *et al.* 2018), there was also an increased response for S3 when it followed a deviant S2 stimulus (M1: p = 0.0001; M2: p = 3.17 * 10^{-27}; Figure 4A & C). S3 is not predicted by S2 when the latter is a deviant but is predicted by S1 in both sorts of triplets. The presence of the

increased response to S3 when it follows a deviant agrees with previous findings that showed that IT neurons respond to temporally adjacent dependencies, i.e. stimulus pairs, but not to non-adjacent dependencies (Meyer *et al.* 2014; Kaposvari *et al.* 2018). As expected from our experimental design, the IT responses to S1 did not differ between the fixed and deviant triplets (M1: $p = 0.73$; M2: $p = 0.87$) and a repeated-measures ANOVA showed a significant interaction of stimulus order and triplet condition in each monkey (M1: $F(1.5, 221.9) = 28.1$, $p = 1.5 * 10^{-9}$; M2: $F(1.5, 246.2) = 213.0$, $p = 2.9 * 10^{-45}$).

Visually-driven MUA was present in the VLPFC area from which we recorded (Figure 4B & D). In both monkeys, the temporal response pattern in VLPFC differed from that observed for the same stimuli in the simultaneously recorded IT, showing a gradual increase of the overall response during the trial for both sorts of triplets. Importantly, VLPFC responses differed between the deviant and fixed triplets, demonstrating an effect of statistical learning in VLPFC (Figure 4B & D). Indeed, a repeated-measures ANOVA showed a significant interaction of stimulus order and triplet condition in each monkey (M1: $F(1.8, 285.6) = 51.5$, $p = 5.4*10^{-18}$, N = 164 units; M2: $F(1.99, 354.3) = 34.9$, $p = 1.4 * 10^{-14}$, N = 179). Whereas there was no difference in response between the two sorts of triplets for S1 (Wilcoxon signed-rank test; M1: $p = 0.43$; M2: $p = 0.55$), the response to S2 was significantly greater for the deviant compared to the fixed triplets in each monkey's VLPFC (M1: $p = 1.6*10^{-8}$; M2: $p = 2.7*10^{-13}$). Similar to IT, we observed an increased response to S3 when it followed a deviant (M1: $p= 2.2*10^{-15}$; M2: $p = 2.0*10^{-11}$). The difference in response in VLPFC between S3 images in the deviant and the fixed S3 triplets was similar to that for S2, especially for M2 (Figure 5 B&D). Thus, in the present design we found no evidence for a sensitivity to non-adjacent dependencies of VLPFC neurons. The VLPFC neurons appear to respond to pairwise image successions, as IT neurons do.

In sum, we obtained similar results in IT and VLPFC: a stronger response to the deviant S2 and S3 when the latter stimulus followed a deviant. Next, we asked whether the deviant response occurred at the same latency in the two areas, or instead whether one area was leading the other. The latency of the mean difference in response to S2 between the deviant and fixed triplets was shorter in IT than in the VLPFC of each monkey (Figure 5). The difference in latency between the two areas of the S2 deviant response (95% confidence interval IT - VLPFC: [-44ms, -88 ms]; data pooled across monkeys (bootstrapping (see Methods))) was significant in each monkey (M1 ($p = 0.005$), M2 ($p < 0.001$); permutation test (see Methods)). Although the difference in latency of the S2 deviant response between VLPFC and IT appears larger in M1 compared to M2 (Figure 5), the latter monkey showed a statistically more reliable effect than the former considering the response variability (see Supplemental Figure S1 for null distributions of the permutation test for each monkey). This was confirmed in an additional analysis in which we estimated the variability of the latency differences with bootstrapping (1000 resamples of units with replacement). We obtained latency estimates in both areas in 95% and 99.5% of the resamples in M1 and M2, respectively. For those samples, the mean difference in deviant response latency (IT – VLPFC) divided by the standard deviation of the difference was -1.5 and -2 in M1 and M2, respectively. The combined data of both monkeys indicates that the deviant response for S2 in IT is not inherited from VLPFC, since it started earlier in IT than in VLPFC.

LFP power

Previous electrophysiological studies on visual sequence learning in macaques showed differences in event-related LFPs between the deviant and fixed sequences (Meyer and Olson

2011; Meyer *et al.* 2014). However, event-related LFPs reflect mainly low frequencies. Thus, it was unknown how the differences in LFP power between deviant and fixed sequences are structured in the time-frequency domain and whether that differs between S2 and S3 stimuli following a deviant. To address this gap and to compare the LFP power to deviants versus fixed sequences between IT and VLPFC, we computed spectral power, using Morlet wavelets, as a function of time and frequency for the deviant and fixed triplet trials (see Methods). The LFP power was averaged across trials and channels for each penetration, thus obtaining a time-frequency power matrix for each daily penetration.

In both monkeys, the LFP power for frequencies above 30-40 Hz was significantly greater for S2 and S3 in the deviant compared to the fixed triplets for IT (Figure 6A&C). However, for lower frequencies, upwards of about 10 Hz, the response for S2 and S3 was significantly smaller in the deviant triplets. In fact, for those lower frequencies, the deviant and the subsequent S3 image produced a stronger suppression of the response than the same images when these were part of a fixed triplet (Figure 6A & C). Although the temporal pattern of the power for the triplets differed between IT and VLPFC, the latter area also showed a significantly increased power for the high frequencies for S2 and S3 in the deviant compared to the fixed triplets in each monkey (Figure 6B & D). For the lower frequencies between about 10 and 40 Hz, the power in VLPFC of each monkey was significantly stronger suppressed by S2 in the deviant compared to the fixed sequence, and such significantly increased suppression was also present for S3 following the deviant in M1 (Figure 6B & D). In addition, we observed in the VLPFC of each monkey an enhanced power in the deviant compared to fixed triplets for delta frequencies (Figure 6B & D).

We compared the timecourse of the difference in power for the deviant relative to the fixed triplets for the high-gamma (51-80 Hz) and beta bands (12-30 Hz; Figure 7) between the two areas for each monkey. We show these bands because higher frequencies typically correlate well with spiking activity and the timecourse of the power for even lower frequency bands is difficult to interpret because of the limited temporal resolution of the Morlet wavelets for these bands. For the high-gamma band, the power was significantly higher in IT for S2 (M1: $p = 0.001$, N = 28 sessions; M2: $p = 0.00002$; N = 24; Wilcoxon signed-rank test) and S3 following a deviant (M1: $p = 0.002$; M2: $p = 0.00002$), whereas no difference in power was observed for S1 (M1: $p = 0.10$; M2: $p = 0.90$) as expected. The same significant effects were observed for VLPFC for that frequency band: an enhanced response for the S2 deviant (M1: $p = 0.000004$; M2: $p = 0.00006$) and S3 following a deviant (M1: $p = 0.00002$; M2: $p = 0.00006$), and no difference in power for S1 (M1: $p = 0.84$; M2: $p = 0.87$). In both monkeys, the deviant response tended to occur earlier in IT than in VLPFC (Figure 7B & D). Also, in both areas, the difference in high-gamma band power between the two sorts of triplets was similar for S2 and S3, showing encoding of temporal adjacent stimulus dependencies.

The beta band showed a significantly decreased power in IT for the S2 deviant (M1: $p = 0.0001$; M2: $p = 0.00002$) and S3 following a deviant (M1: $p = 0.002457$; M2: $p = 0.000021$), but there was no difference between the two sorts of triplets for S1 (M1: $p = 0.48$; M2: $p = 0.36$; Figure 7A & C). The same effects were observed for the beta power in VLPFC: significant differences in power between the two sorts of triplets for S2 (M1: $p = 0.000005$; M2: $p = 0.00002$) and S3 (M1: $p= 0.000015$; M2: $p = 0.001$) but not S1 (M1: $p = 0.72$; M2: $p = 0.49$). Note that in this analysis, M2 showed a significant effect for S3 in the beta band while that failed to reach significance in the time-frequency plot (Figure 6) when applying a correction for multiple comparisons at the cluster level. Thus, overall, the enhanced suppression of the beta band

demonstrated also encoding of temporal adjacent dependencies, as did the high-gamma band and the MUA. That said, there was a trend, especially in M2, for a greater difference in the beta band power between the two sorts of triplets for S2 compared to S3 (Figure 7A & C). Across monkeys, there was no consistent difference in onset of the deviant response between the two areas for these low frequencies (Figure 7A & C).

In sum, the LFP power analysis supported a deviant response in IT and VLPFC, for both S2 and S3 following a deviant. The sign of the deviant response (enhancement versus suppression) was opposite in high (supra-gamma) and low-frequency bands (beta; low-gamma). Both areas thus showed encoding of temporal regularities based on transition probabilities.

Granger causality

Granger Causality analysis can be employed to estimate the directed information flow between areas. It is a correlation-based method in which one assesses to what extent the LFP signal in one area can be predicted better when considering the signal in the other area. We computed Granger Causality (GC) for the fixed and deviant triplet trials. However, the GC values for the deviant triplets were rather noisy, especially in M1, likely because of the low number of trials per daily session, and will not be described here. For the fixed triplet trials, GC was inconsistent across monkeys for the IT to VLPFC direction (Figure 8A & D). The statistically significant GC in the high-gamma band observed for the latter direction in M1 did not survive time-reversed GC testing (see Methods) and thus we cannot exclude that this is a spurious effect. For the fixed triplet trials, we observed significant GC in the low-frequency band between 20 and 40 Hz for the VLPFC to IT direction (Figure 8B & E). The dominant direction of information flow in this low-frequency band was from VLPFC to IT (Figure 8C & F),

although this was prominent only during the fixation period before and after the triplet presentation in M2. To appreciate better the timecourse of the GC values for these low frequencies, we plot the mean GC values within this band during the trial in Figure 9. In both monkeys, the image onsets resulted in a reduction of the GC values in the low-frequency band for both directions (Figure 9A & D; Figure 9B & E). Note that S1 and S2 can predict the subsequent image in the fixed triplets whereas S3 does not predict an image. However, there was no evidence for such a flow of predictions from VLPFC to IT in the timecourse of the low-frequency band GC values (Figure 9B &E): the changes in GC values were similar for the three subsequent images. Indeed, the low-frequency GC in that direction appeared to be mainly image-driven.

Discussion

We recorded multi-unit spiking activity and LFPs in macaque IT and VLPFC after the animals were exposed to triplets of visual images of which the presentation order was fixed ("fixed triplets"). The MUA in IT was stronger to images that violated the learned sequence compared to the same images presented in the learned triplets, in agreement with previous studies (Meyer and Olson 2011; Schwiedrzik and Freiwald 2017; Kaposvari *et al.* 2018), and we show now that this also holds for VLPFC. In both cortical areas, the high-gamma LFP power showed an enhanced response to the deviants while the beta power showed a suppressed response to the deviant stimuli, compared to the fixed triplets. The enhanced MUA and high-gamma LFP power were present not only for the deviant image but also for the image following the deviant. This agrees with previous studies showing sensitivity for temporal adjacent dependencies in IT at the spiking level (Meyer *et al.* 2014; Kaposvari *et al.* 2018) and we

demonstrate here that the same is true for VLPFC. Furthermore, we show that the response to the deviant image occurs later in VLPFC than in IT, suggesting that at least the early phase of the deviant response in IT is not inherited from VLPFC. These data support predictive coding theories that propose a feedforward flow of prediction errors (Friston 2005).

Using a similar paradigm as (Meyer and Olson 2011), enhanced activation to deviant image doublets has been observed with fMRI in the human occipito-temporal cortex (Richter *et al.* 2018; Richter and de Lange 2019). However, using a stimulus paradigm that is similar to ours, fMRI activations to the deviants were absent in the frontal cortex when the stimuli were not task-relevant (Richter *et al.* 2018). In a subsequent human fMRI study, frontal activations were present when the subjects had to categorize the predictable trailing images and hence were task-relevant when measuring activations to deviants (Richter and de Lange 2019). In our paradigm, the monkeys were performing a passive fixation task during the recordings, and image identity was task-irrelevant. Hence, our data demonstrate that a deviant response is present at the neural level in the prefrontal cortex even when image identity is task-irrelevant.

Our data show for the first time that macaque VLPFC neurons distinguish sequences that differ only in learned transition probabilities. A recent study reported increased MUA and high-gamma band LFP responses in macaque lateral prefrontal cortex and other cortical areas when images were presented as a sample in randomly ordered delayed matching to sample trials compared to when the same image was repeated as a sample in blocks of 50 trials (Bastos et al. 2020). In that study, prediction was manipulated by stimulus repetition. However, it is known that repetition induces processes that can be dissociated from prediction, such as repetition suppression and reduced attention to the repeated sample stimuli (Vinken and Vogels 2017; Vinken et al. 2018; Feuerriegel *et al.* 2021), which makes interpretation of the

reported effects reported by (Bastos *et al.* 2020) in terms of prediction not straightforward. In fact, single-unit studies that control for repetition suppression found little or no evidence in macaque IT (Kaliukhovich and Vogels 2014), V1 and V4 (Solomon et al. 2021) for prediction-related effects when employing task-irrelevant repeated stimuli in short blocks of trials, unlike the robust IT (and VLPFC) responses to deviants after longer exposure to fixed stimulus sequences (Meyer and Olson 2011; Schwiedrzik and Freiwald 2017; Kaposvari *et al.* 2018).

A recent human intracranial field potential study provided evidence for the encoding of transition probabilities of sequences of randomly ordered image pairs in several brain areas, including occipito-temporal and frontal cortex (Henin et al. 2021). However, unlike in the present macaque study, such sensitivity for transition probabilities was not observed in the high-gamma power, being evident only in the low-frequencies in that study. The cause of this discrepancy between our and the human study might be related to the different recording techniques, i.e. intracortical microelectrode versus electrocorticographic macroelectrode recordings, although one cannot exclude differences in the amount of exposure to the stimulus regularities, which was more prolonged in our study, or, but even less likely a species difference.

In line with other studies of visual statistical learning in humans (Alamia et al. 2019; Richter and de Lange 2019) and monkeys (Schwiedrzik and Sudmann 2020), pupil size measures differed between deviant and fixed triplets, providing a behavioral correlate of visual statistical learning in our monkey subjects. The onset of the deviant responses in IT and VLPFC was much earlier than the latency of the pupil response, indicating that the deviant response in these areas is not caused by the variation in pupil size and concomitant changes in retinal illuminance.

In both IT and VLPFC, the deviant produced increased gamma-band responses and decreased beta-band responses. The increase in high-gamma band power in both areas to the deviant stimulus is not surprising given the often-observed correlation between MUA and high-gamma band power. The higher power for the fixed compared to the deviant triplets in the beta-band is reminiscent of the typically observed increased beta-band power for a repeated, adapted stimulus, whereas repetition produces a decreased gamma power ((Kaliukhovich and Vogels 2011, 2012; Vinken *et al.* 2018); but see De Baene and Vogels 2010). This may relate to a higher saliency of non-repeated and deviant stimuli in the stimulus sequences, since more salient stimuli, e.g. with a higher signal-to-noise ratio, produce a stronger suppression of beta-power in extrastriate areas (Verhoef et al. 2011).

Beta-band activity has been related to feedback (Bastos et al. 2015). We found in both VLPFC and IT, two areas arguably at different hierarchical stages, a greater beta-band power for the fixed, predictable images, which then would imply that in both areas feedback is increased in the fixed sequence. In each animal and area, the beta-band activity tended to be larger at the end of the first and the second image of the fixed triplet, i.e. when the next image can be predicted, than for the third image of the triplet, which does not predict a successive image (Figure 6). This is consistent with the idea that beta-band activity relates to predictive feedback (Mohanta et al. 2021), although this is rather indirect evidence and speculative. The Granger causality analysis suggested a dominant directional information flow from VLPFC to IT for the beta to low-gamma frequencies, which is in line with feedback from VLPFC to IT. However, similar to previous observations for the lateral intraparietal cortex to IT information flow (Verhoef *et al.* 2011), the GC values in the low-frequency bands for the VLPFC to IT direction were highest during the pre-stimulus baseline and reduced during stimulus presentation, especially in M2. Overall, the GC VLPFC-to-IT information flow in the low-

frequency bands appeared to follow the image presentations, irrespective of their predictive status. Further work in which one compares GC in the low-frequency bands between fixed-order image sequences and sequences in which the images are presented in random order, hence are unpredictable, may shed light on the significance of the low-frequency bands in the context of predictive feedback for visual processing.

In VLPFC, but not IT, we observed enhanced LFP power to the deviants for very low frequencies in the delta range. Although such a very low spectral frequency band activity has been implied in cognitive functions such as decision making (Nacher et al. 2013) and is informative about visual stimulus identity, at least in the primary visual cortex (Belitski et al. 2008), the significance of these very slow oscillations in VLPFC in predictive processing or deviance detection is unclear.

Overall, the deviant response was similar in VLPFC and IT, both for MUA and LFP power, except for the delta band. This was also the case for the response to the stimulus trailing the deviant which showed an enhanced response compared to the fixed triplets. Thus, as for IT neurons (Meyer *et al.* 2014; Kaposvari *et al.* 2018), the response to the deviant was similar in magnitude to the response to the stimulus following the deviant for macaque VLPFC neurons which is in line with encoding of the relationship between two successive stimuli. Despite the absence of evidence for encoding of non-adjacent dependencies in the present study, we cannot exclude that in the context of other sequences or tasks, the neurons will be sensitive to non-adjacent dependencies in VLPFC. Indeed, it is possible that our monkeys did simply not learn non-adjacent dependencies but only successive pairs in our task.

Although qualitative characteristics of the deviant response were similar between IT and VLPFC, the deviant response for S2 had an earlier onset in IT compared to VLPFC. This implies

that the deviant response in IT, at least in its early phase, does not result from deviance detection in VLPFC. Indeed, it is inconsistent with the hypothesis that the VLPFC detects the difference between the expected and presented stimulus and then sends the mismatch signal to IT. Also, the earlier onset of the deviant response in IT is not in line with theories that propose a top-down flow of prediction errors (Heeger 2017). Furthermore, the difference in onset latency of the deviant response between IT and VLPFC renders it unlikely that the deviant response in these areas results merely from a common mismatch (e.g. arousal or saliency) signal, originating for instance from basal forebrain neurons that also show evidence of deviant responses in the monkey (Zhang et al. 2019). The later onset of the deviant response in VLPFC compared to IT is in line with the idea that it originates in the visual cortex and is then transmitted to VLPFC. Thus, our findings are consistent with predictive coding theories that propose a feedforward flow of prediction errors that are generated in hierarchically lower cortical areas (Friston 2005).

Funding

This research was supported by Fonds voor Wetenschappelijk Onderzoek (FWO) Vlaanderen (G088418N) and KU Leuven grants C14/17/109 and C14/21/111. R.V and R.R were supported by the European Research Council (ERC) under the European Union's Horizon 2020 research and innovation programme (grant agreement No. 856495).

Acknowledgments.

The authors thank A. Coeman, C. Fransen, P. Kayenbergh, I. Puttemans, A. Hermans, G. Meulemans, W. Depuydt, C. Ulens, S. Verstraeten, and M. Depaep for technical and administrative support. Dr. V. Vergnieux conducted the monkey fMRI studies that lead to the electrophysiological experiments reported in this paper and contributed to the recordings of one monkey.

References

Aizenstein HJ, Stenger VA, Cochran J, Clark K, Johnson M, Nebes RD, Carter CS. 2004. Regional brain activation during concurrent implicit and explicit sequence learning. Cereb Cortex. 14:199-208.
Alamia A, VanRullen R, Pasqualotto E, Mouraux A, Zenon A. 2019. Pupil-Linked Arousal Responds to Unconscious Surprisal. J Neurosci. 39:5369-5376.
Bastos AM, Lundqvist M, Waite AS, Kopell N, Miller EK. 2020. Layer and rhythm specificity for predictive routing. Proc Natl Acad Sci U S A. 117:31459-31469.
Bastos AM, Schoffelen JM. 2015. A Tutorial Review of Functional Connectivity Analysis Methods and Their Interpretational Pitfalls. Front SystNeurosci. 9:175.
Bastos AM, Vezoli J, Bosman CA, Schoffelen JM, Oostenveld R, Dowdall JR, De Weerd P, Kennedy H, Fries P. 2015. Visual areas exert feedforward and feedback influences through distinct frequency channels. Neuron. 85:390-401.
Belitski A, Gretton A, Magri C, Murayama Y, Montemurro MA, Logothetis NK, Panzeri S. 2008. Low-frequency local field potentials and spikes in primary visual cortex convey independent visual information. JNeurosci. 28:5696-5709.
Bullier J, Schall JD, Morel A. 1996. Functional streams in occipito-frontal connections in the monkey. Behav Brain Res. 76:89-97.
Camalier CR, Scarim K, Mishkin M, Averbeck BB. 2019. A Comparison of Auditory Oddball Responses in Dorsolateral Prefrontal Cortex, Basolateral Amygdala, and Auditory Cortex of Macaque. J Cogn Neurosci. 31:1054-1064.
Caprara I, Premereur E, Romero MC, Faria P, Janssen P. 2018. Shape responses in a macaque frontal area connected to posterior parietal cortex. Neuroimage. 179:298-312.
Chao ZC, Takaura K, Wang L, Fujii N, Dehaene S. 2018. Large-Scale Cortical Networks for Hierarchical Prediction and Prediction Error in the Primate Brain. Neuron. 100:1252-1266 e1253.
Cohen MX. 2014. Analyzing Neural Time Series Data. Theory and Practice. Cambridge, MA: MIT Press.
De Baene W, Vogels R. 2010. Effects of adaptation on the stimulus selectivity of macaque inferior temporal spiking activity and local field potentials. CerebCortex. 20:2145-2165.
Dehaene S, Meyniel F, Wacongne C, Wang L, Pallier C. 2015. The Neural Representation of Sequences: From Transition Probabilities to Algebraic Patterns and Linguistic Trees. Neuron. 88:2-19.
Denys K, Vanduffel W, Fize D, Nelissen K, Sawamura H, Georgieva S, Vogels R, Van ED, Orban GA. 2004. Visual activation in prefrontal cortex is stronger in monkeys than in humans. JCogn Neurosci. 16:1505-1516.
Dhamala M, Rangarajan G, Ding M. 2008. Analyzing information flow in brain networks with nonparametric Granger causality. Neuroimage. 41:354-362.
Ding M, Bressler SL, Yang W, Liang H. 2000. Short-window spectral analysis of cortical event-related potentials by adaptive multivariate autoregressive modeling: data preprocessing, model validation, and variability assessment. Biol Cybern. 83:35-45.
Durschmid S, Edwards E, Reichert C, Dewar C, Hinrichs H, Heinze HJ, Kirsch HE, Dalal SS, Deouell LY, Knight RT. 2016. Hierarchy of prediction errors for auditory events in human temporal and frontal cortex. Proc Natl Acad Sci U S A. 113:6755-6760.
Ebitz RB, Pearson JM, Platt ML. 2014. Pupil size and social vigilance in rhesus macaques. Front Neurosci. 8:100.
Ekstrom LB, Roelfsema PR, Arsenault JT, Bonmassar G, Vanduffel W. 2008. Bottom-up dependent gating of frontal signals in early visual cortex. Science. 321:414-417.
Feuerriegel D, Vogels R, Kovacs G. 2021. Evaluating the evidence for expectation suppression in the visual system. Neurosci Biobehav Rev. 126:368-381.
Friston K. 2005. A theory of cortical responses. PhilosTransRSocLond B BiolSci. 360:815-836.
Giarrocco F, Averbeck BB. 2021. Organization of parietoprefrontal and temporoprefrontal networks in the macaque. J Neurophysiol. 126:1289-1309.
Heeger DJ. 2017. Theory of cortical function. Proc Natl Acad Sci U S A. 114:1773-1782.

Henin S, Turk-Browne NB, Friedman D, Liu A, Dugan P, Flinker A, Doyle W, Devinsky O, Melloni L. 2021. Learning hierarchical sequence representations across human cortex and hippocampus. Sci Adv. 7.
Kaliukhovich DA, Vogels R. 2011. Stimulus repetition probability does not affect repetition suppression in macaque inferior temporal cortex. CerebCortex. 21:1547-1558.
Kaliukhovich DA, Vogels R. 2012. Stimulus repetition affects both strength and synchrony of macaque inferior temporal cortical activity. JNeurophysiol. 107:3509-3527.
Kaliukhovich DA, Vogels R. 2014. Neurons in macaque inferior temporal cortex show no surprise response to deviants in visual oddball sequences. JNeurosci. 34:12801-12815.
Kaposvari P, Kumar S, Vogels R. 2018. Statistical Learning Signals in Macaque Inferior Temporal Cortex. Cereb Cortex. 28:250-266.
Kravitz DJ, Saleem KS, Baker CI, Ungerleider LG, Mishkin M. 2013. The ventral visual pathway: an expanded neural framework for the processing of object quality. Trends Cogn Sci. 17:26-49.
Krogh L, Vlach HA, Johnson SP. 2012. Statistical learning across development: flexible yet constrained. Front Psychol. 3:598.
Kumar S, Kaposvari P, Vogels R. 2017. Encoding of Predictable and Unpredictable Stimuli by Inferior Temporal Cortical Neurons. J Cogn Neurosci. 29:1445-1454.
Li N, Dicarlo JJ. 2008. Unsupervised natural experience rapidly alters invariant object representation in visual cortex. Science. 321:1502-1507.
Manahova ME, Mostert P, Kok P, Schoffelen JM, de Lange FP. 2018. Stimulus Familiarity and Expectation Jointly Modulate Neural Activity in the Visual Ventral Stream. J Cogn Neurosci. 30:1366-1377.
Markov NT, Ercsey-Ravasz MM, Gomes ARR, Lamy C, Magrou L, Vezoli J, Misery P, Falchier A, Quilodran R, Gariel MA, Sallet J, Gamanut R, Huissoud C, Clavagnier S, Giroud P, Sappey-Marinier D, Barone P, Dehay C, Toroczkai Z, Knoblauch K, Van Essen DC, Kennedy H. 2014. A Weighted and Directed Interareal Connectivity Matrix for Macaque Cerebral Cortex. Cerebral Cortex. 24:17-36.
Meyer T, Olson CR. 2011. Statistical learning of visual transitions in monkey inferotemporal cortex. Proc Natl Acad Sci U S A. 108:19401-19406.
Meyer T, Ramachandran S, Olson CR. 2014. Statistical learning of serial visual transitions by neurons in monkey inferotemporal cortex. J Neurosci. 34:9332-9337.
Mohanta S, Afrasiabi M, Casey CP, Tanabe S, Redinbaugh MJ, Kambi NA, Phillips JM, Polyakov D, Filbey W, Austerweil JL, Sanders RD, Saalmann YB. 2021. Predictive Feedback, Early Sensory Representations, and Fast Responses to Predicted Stimuli Depend on NMDA Receptors. J Neurosci. 41:10130-10147.
Nacher V, Ledberg A, Deco G, Romo R. 2013. Coherent delta-band oscillations between cortical areas correlate with decision making. Proc Natl Acad Sci U S A. 110:15085-15090.
Nourski KV, Steinschneider M, Rhone AE, Kawasaki H, Howard MA, 3rd, Banks MI. 2018. Processing of auditory novelty across the cortical hierarchy: An intracranial electrophysiology study. Neuroimage. 183:412-424.
Oostenveld R, Fries P, Maris E, Schoffelen JM. 2011. FieldTrip: Open source software for advanced analysis of MEG, EEG, and invasive electrophysiological data. Comput Intell Neurosci. 2011:156869.
Pagliaccio D, Pine DS, Leibenluft E, Dal Monte O, Averbeck BB, Costa VD. 2019. Cross-species convergence in pupillary response: understanding human anxiety via non-human primate amygdala lesion. Soc Cogn Affect Neurosci. 14:591-599.
Pagnotta MF, Dhamala M, Plomp G. 2018. Benchmarking nonparametric Granger causality: Robustness against downsampling and influence of spectral decomposition parameters. Neuroimage. 183:478-494.
Peter A, Stauch BJ, Shapcott K, Kouroupaki K, Schmiedt JT, Klein L, Klon-Lipok J, Dowdall JR, Scholvinck ML, Vinck M, Schmid MC, Fries P. 2021. Stimulus-specific plasticity of macaque V1 spike rates and gamma. Cell Rep. 37:110086.
Popivanov ID, Jastorff J, Vanduffel W, Vogels R. 2014. Heterogeneous Single-Unit Selectivity in an fMRI-Defined Body-Selective Patch. Journal of Neuroscience. 34:95-111.

Ramachandran S, Meyer T, Olson CR. 2016. Prediction suppression in monkey inferotemporal cortex depends on the conditional probability between images. J Neurophysiol. 115:355-362.
Ramachandran S, Meyer T, Olson CR. 2017. Prediction suppression and surprise enhancement in monkey inferotemporal cortex. J Neurophysiol. 118:374-382.
Richter D, de Lange FP. 2019. Statistical learning attenuates visual activity only for attended stimuli. Elife. 8.
Richter D, Ekman M, de Lange FP. 2018. Suppressed Sensory Response to Predictable Object Stimuli throughout the Ventral Visual Stream. J Neurosci. 38:7452-7461.
Riley MR, Qi XL, Constantinidis C. 2017. Functional specialization of areas along the anterior-posterior axis of the primate prefrontal cortex. Cereb Cortex. 27:3683-3697.
Rosenthal CR, Andrews SK, Antoniades CA, Kennard C, Soto D. 2016. Learning and Recognition of a Non-conscious Sequence of Events in Human Primary Visual Cortex. Curr Biol. 26:834-841.
Rosenthal CR, Mallik I, Caballero-Gaudes C, Sereno MI, Soto D. 2018. Learning of goal-relevant and -irrelevant complex visual sequences in human V1. Neuroimage. 179:215-224.
Sakai K, Miyashita Y. 1991. Neural organization for the long-term memory of paired associates. Nature. 354:152-155.
Saleem KS, Miller B, Price JL. 2014. Subdivisions and connectional networks of the lateral prefrontal cortex in the macaque monkey. J Comp Neurol. 522:1641-1690.
Schwiedrzik CM, Freiwald WA. 2017. High-Level Prediction Signals in a Low-Level Area of the Macaque Face-Processing Hierarchy. Neuron. 96:89-97.e84.
Schwiedrzik CM, Sudmann SS. 2020. Pupil Diameter Tracks Statistical Structure in the Environment to Increase Visual Sensitivity. J Neurosci. 40:4565-4575.
Sereno AB, Maunsell JH. 1998. Shape selectivity in primate lateral intraparietal cortex. Nature. 395:500-503.
Seth AK. 2010. A MATLAB toolbox for Granger causal connectivity analysis. J Neurosci Methods. 186:262-273.
Solomon SS, Tang H, Sussman E, Kohn A. 2021. Limited Evidence for Sensory Prediction Error Responses in Visual Cortex of Macaques and Humans. Cereb Cortex. 31:3136-3152.
Srivastava S, Orban GA, De Maziere PA, Janssen P. 2009. A distinct representation of three-dimensional shape in macaque anterior intraparietal area: fast, metric, and coarse. JNeurosci. 29:10613-10626.
Turk-Browne NB. 2012. Statistical learning and its consequences. NebrSympMotiv. 59:117-146.
Vergnieux V, Vogels R. 2020. Statistical Learning Signals for Complex Visual Images in Macaque Early Visual Cortex. Front Neurosci. 14:789.
Verhoef BE, Kayaert G, Franko E, Vangeneugden J, Vogels R. 2008. Stimulus similarity-contingent neural adaptation can be time and cortical area dependent. JNeurosci. 28:10631-10640.
Verhoef BE, Vogels R, Janssen P. 2011. Synchronization between the end stages of the dorsal and the ventral visual stream. JNeurophysiol. 105:2030-2042.
Vinken K, Op de Beeck HP, Vogels R. 2018. Face Repetition Probability Does Not Affect Repetition Suppression in Macaque Inferotemporal Cortex. J Neurosci. 38:7492-7504.
Vinken K, Vogels R. 2017. Adaptation can explain evidence for encoding of probabilistic information in macaque inferior temporal cortex. Curr Biol. 27:R1210-R1212.
Webster MJ, Bachevalier J, Ungerleider LG. 1994. Connections of inferior temporal areas TEO and TE with parietal and frontal cortex in macaque monkeys. CerebCortex. 4:470-483.
Willenbockel V, Sadr J, Fiset D, Horne GO, Gosselin F, Tanaka JW. 2010. Controlling low-level image properties: the SHINE toolbox. Behav Res Methods. 42:671-684.
Wilson B, Kikuchi Y, Sun L, Hunter D, Dick F, Smith K, Thiele A, Griffiths TD, Marslen-Wilson WD, Petkov CI. 2015. Auditory sequence processing reveals evolutionarily conserved regions of frontal cortex in macaques and humans. Nat Commun. 6:8901.
Wolff A, Berberian N, Golesorkhi M, Gomez-Pilar J, Zilio F, Northoff G. 2022. Intrinsic neural timescales: temporal integration and segregation. Trends Cogn Sci. 26:159-173.

Xu R, Bichot NP, Takahashi A, Desimone R. 2021. The cortical connectome of primate lateral prefrontal cortex. Neuron.
Zhang K, Chen CD, Monosov IE. 2019. Novelty, Salience, and Surprise Timing Are Signaled by Neurons in the Basal Forebrain. Curr Biol. 29:134-142 e133.

Figure Legends

Figure 1. Recording location in IT and VLPFC. Sagittal (IT) and coronal MRI slices (VLPFC) of the brain of M1 (A) and M2 (B). The estimated location of a laminar electrode penetration is indicated by a white line. IT recordings were in the ventral bank of the STS while those in VLPFC were ventral to the principal sulcus and in the anterior bank of the inferior ramus of the arcuate sulcus.

Figure 2. Stimuli and paradigm. A. Five triplets of images of animals presented to monkey M1. The triplets presented to M2 differed from the ones shown here. B. Deviant triplets were created by replacing the second image of the triplet with one of the other second images of the four remaining triplets. In this illustration, the second image of the deviant triplet (red frame) is identical to the image of the fixed triplet (blue frame) presented in the first row of A whereas the first and third image corresponds to the fixed triplet of the second row of A. C. Illustration of a trial. The monkey needed to fixate a red target during the entire trial. The number above the panels indicates the duration of the trial phase. The 3 images of a triplet were presented back-to-back without any interstimulus interval, each for 506 ms after the monkey was fixating the target for 506 ms. The fixation period after the third image had a variable duration after which the monkey was rewarded.

Figure 3. Pupil size. Mean z-scored pupil size for the fixed (dotted line) and deviant (solid line) triplets. 0 indicates the onset of the triplet. Bands indicate 95% confidence intervals. N corresponds to the number of blocks (see Methods). A and B shows the data of M1 and M2, respectively.

Figure 4. Average firing rate (MUA) to fixed (dotted line) and deviant (solid line) triplets. The baseline response in the 280 ms period before triplet onset (indicated by 0) was subtracted

for each condition and unit before averaging the firing rate. Bands indicate 95% confidence intervals. N corresponds to the number of units, obtained in 28 and 24 sessions in M1 and M2, respectively. A & B: population PSTHs of IT (A) and VLPFC (B) in M1. C & D: population PSTHs of IT (C) and VLPFC (D) in M2.

Figure 5. Difference in firing rate between the deviant and fixed triplets. A&C Difference in firing rate between the two triplets for IT (solid line) and VLPFC (dotted line). To facilitate a comparison of the latencies of the onset of the deviant response, the difference in the firing rate of the two conditions was normalized by the maximum difference for each area. Bands indicate 95% confidence intervals of the difference (bootstrapped across units). For each monkey, the dots (arrows) indicate the estimated latencies for IT and VLPFC, respectively, using the procedure described in the Methods. B&D. Difference in firing rate between the deviant and fixed condition for S2 and S3 in VLPFC for M1 and M2. The response difference was normalized as for A &B. 0 corresponds to stimulus onset. Bin width is 11 ms for all panels and the number of MUA units is identical to those in Figure 4.

Figure 6. LFP power for deviant and fixed triplets. In each panel, the upper and middle rows show the time-frequency plots of the normalized LFP power for deviant and fixed triplet, respectively, and the lower row shows the significant differences in power between the deviant and fixed triplets ($p < 0.05$; corrected for multiple comparisons using the cluster-based method; see Methods) as a function of time and frequency. The LFP power in the upper two panels was normalized relative to baseline (see Methods). 0 corresponds to triplet onset and N indicates the number of trials. A & B: LFP power data for IT (A) and VLPFC (B) in M1. C & D: LFP power data for IT (A) and VLPFC (B) in M2. The stippled horizontal lines indicate the borders of the beta and high-gamma bands employed in Figure 7.

Figure 7. Difference in LFP power between the deviant and fixed triplets for IT (solid line) and VLPFC (dotted line). The difference in mean LFP power between the deviant and fixed triplets is plotted as a function of time for the beta band (A&C) and high-gamma bands (B&D) in each monkey. To facilitate the comparison of the deviant response between areas, the difference in mean power was normalized by the maximum difference for each area. Bands indicate 95% confidence intervals of the mean difference (bootstrapped across sessions; N = 28 in M1 and 24 in M2). N indicates the number of sessions.

Figure 8. Time-frequency plots of Granger causality during fixed triplet trials. The first column shows the mean Granger causality values (averaged across channel pairs and then across daily sessions (N = 25 and N = 23 in M1 and M2, respectively; see Methods) for the IT to VLPFC direction for M1 (A) and M2 (D). The second column shows the Granger causality values for the VLPFC to IT direction for M1 (B) and M2 (E). The third column shows the difference in Granger causality between the directions VLPFC to IT – IT to VLPFC. The horizontal lines show the border of the beta-gamma low-frequency band employed for the data of Figure 9.

Figure 9. Granger causality values in the low-frequency band during fixed triplet trials. The first two columns show the mean Granger causality for the 20-40Hz band for the two directions for each monkey. Before averaging, the Granger causality values were z-scored per daily session. The bands show 95% confidence intervals (bootstrapping across daily sessions; same sessions as in Figure 8). The right column shows the mean z-scored difference in Granger causality between the directions VLPFC to IT and IT to VLPFC. A-C: data of M1; D-F: data of M2. Bands show 95% confidence intervals of the mean difference (bootstrapping across sessions).

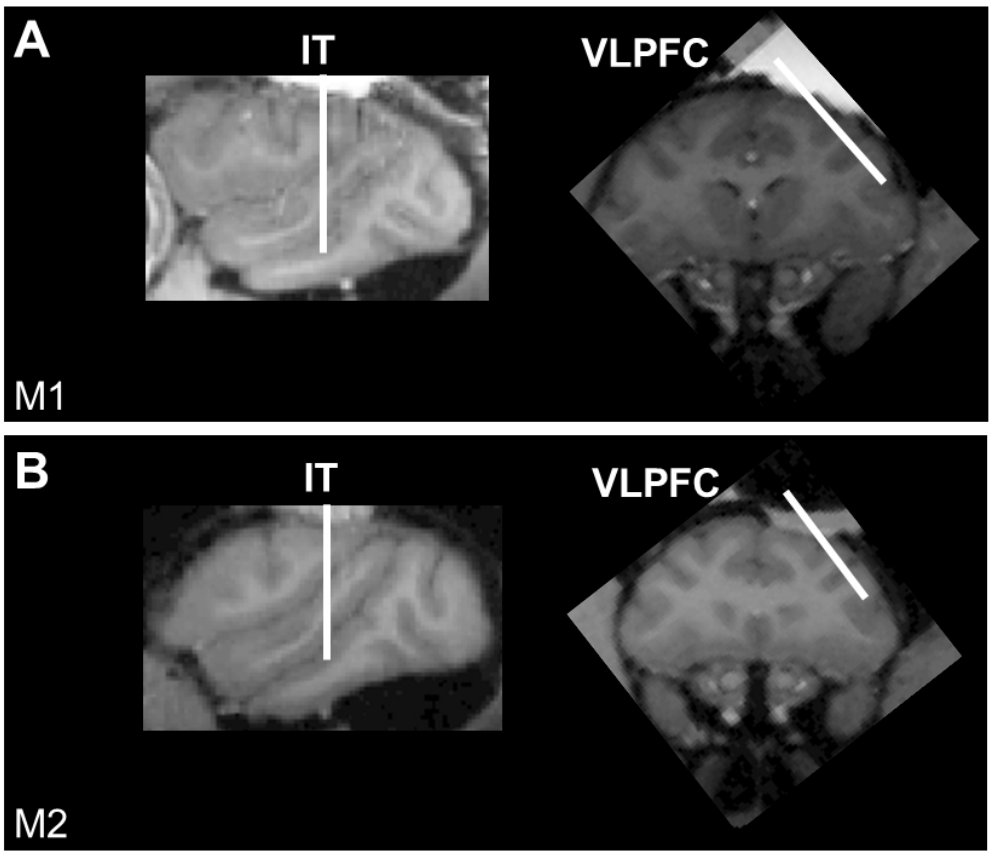

Figure 1

70x62mm (300 x 300 DPI)

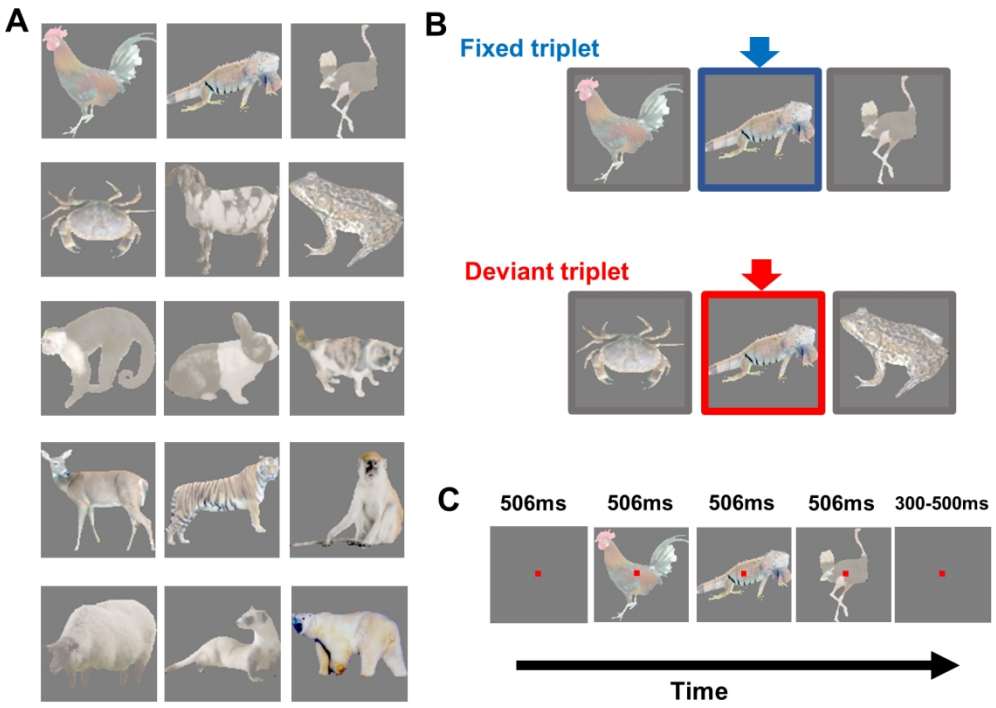

Figure 2

150x109mm (300 x 300 DPI)

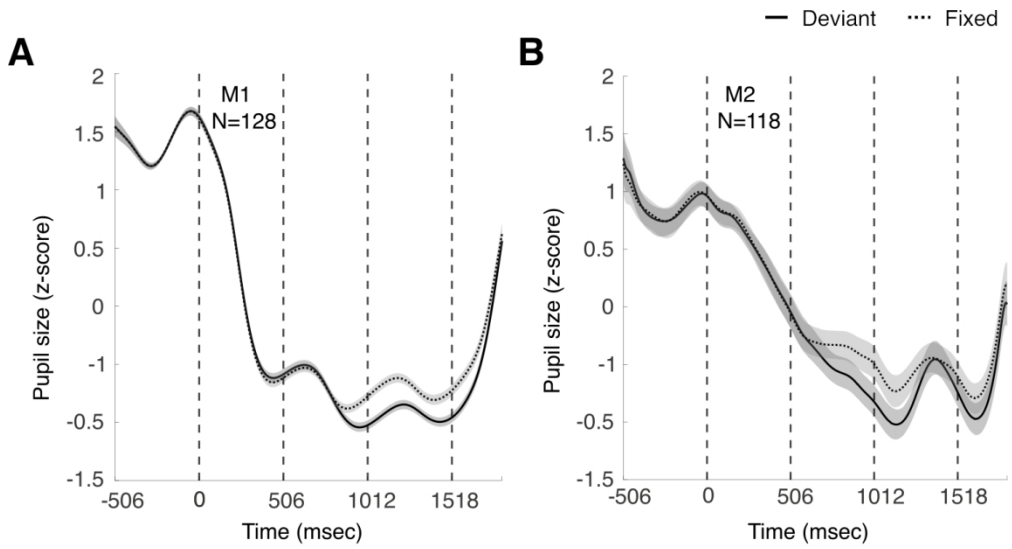

Figure 3

327x175mm (118 x 118 DPI)

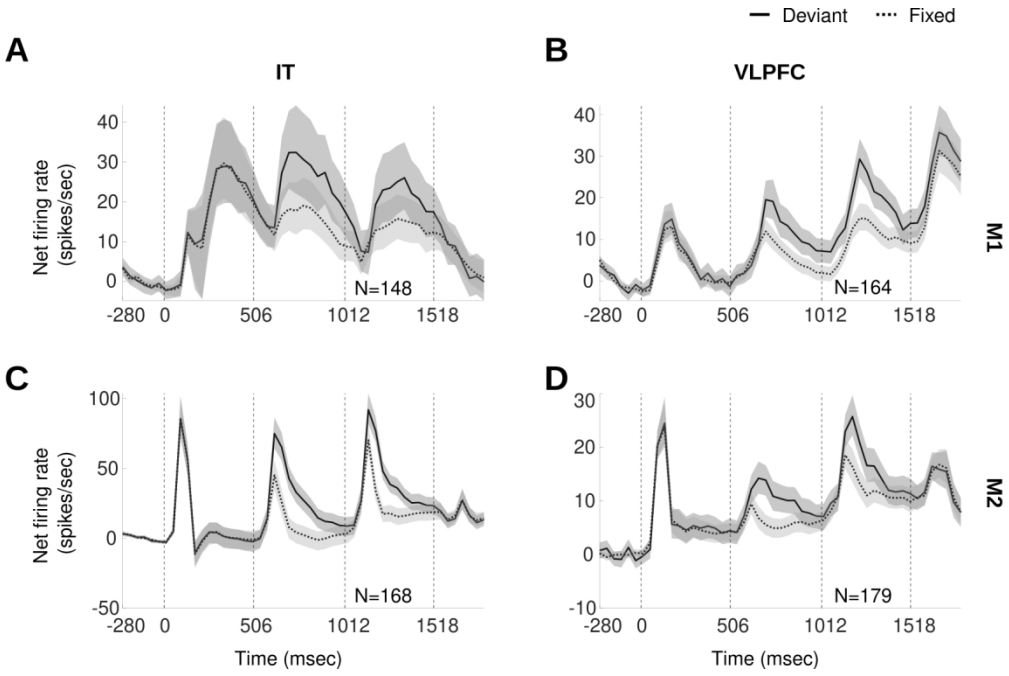

Figure 4

368x243mm (118 x 118 DPI)

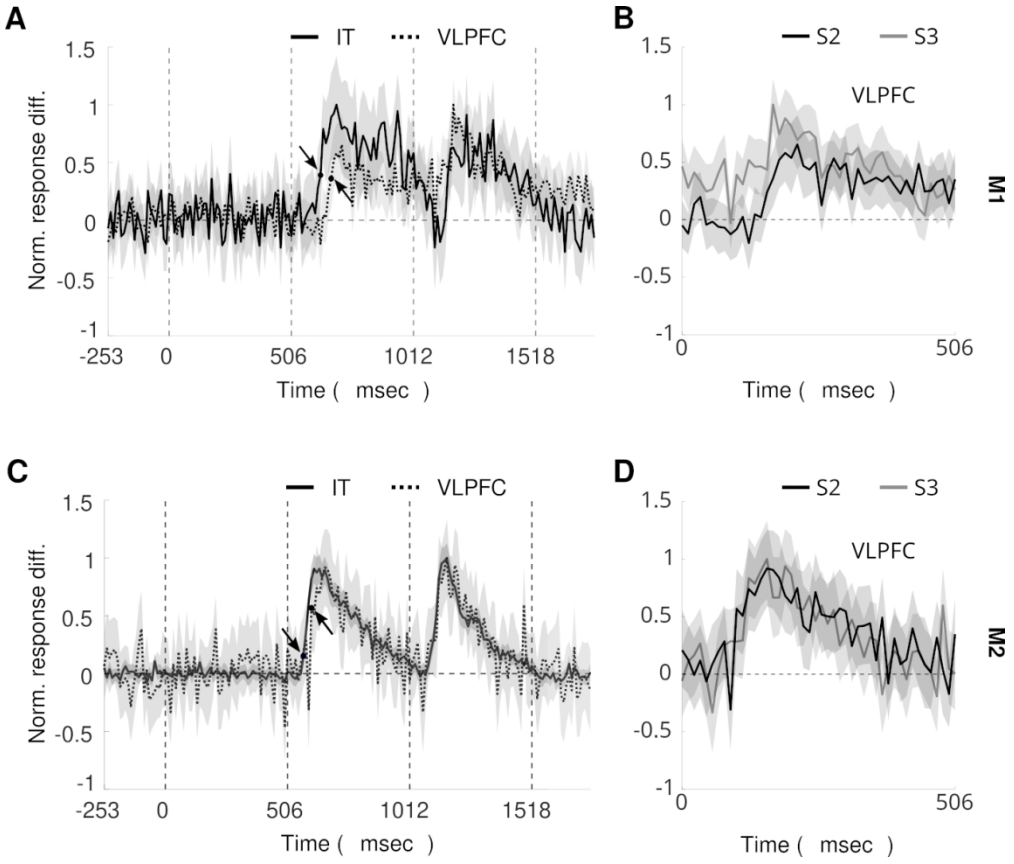

Figure 5

301x256mm (118 x 118 DPI)

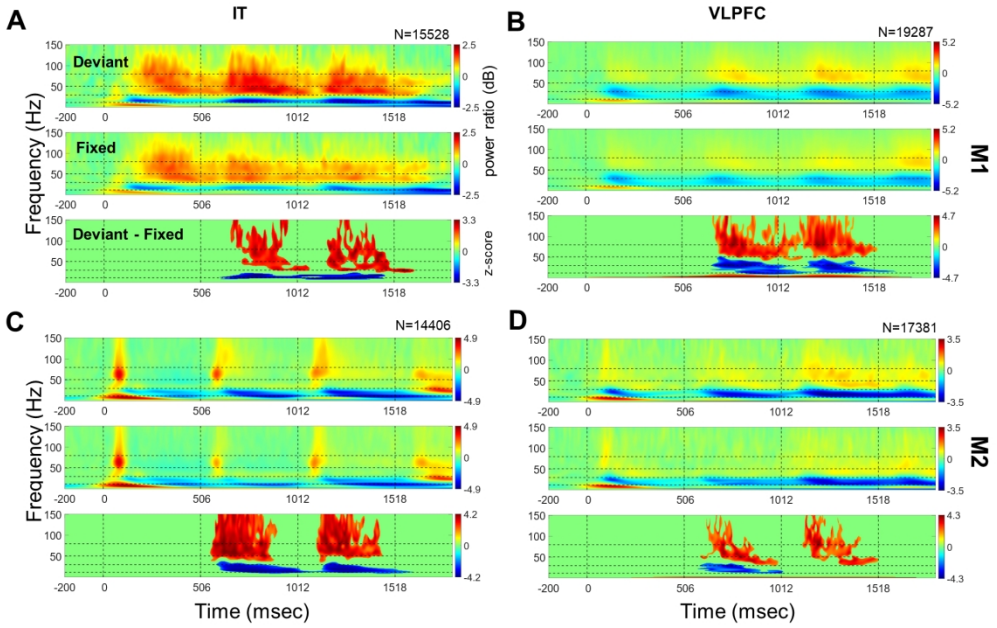

Figure 6

180x119mm (300 x 300 DPI)

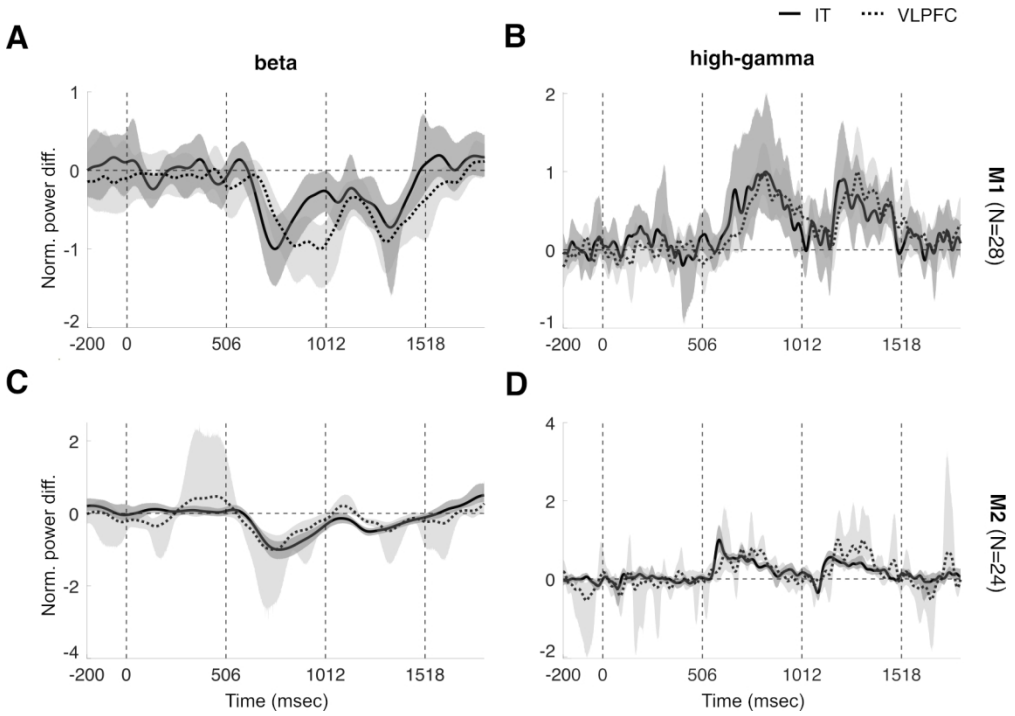

Figure 7

383x269mm (118 x 118 DPI)

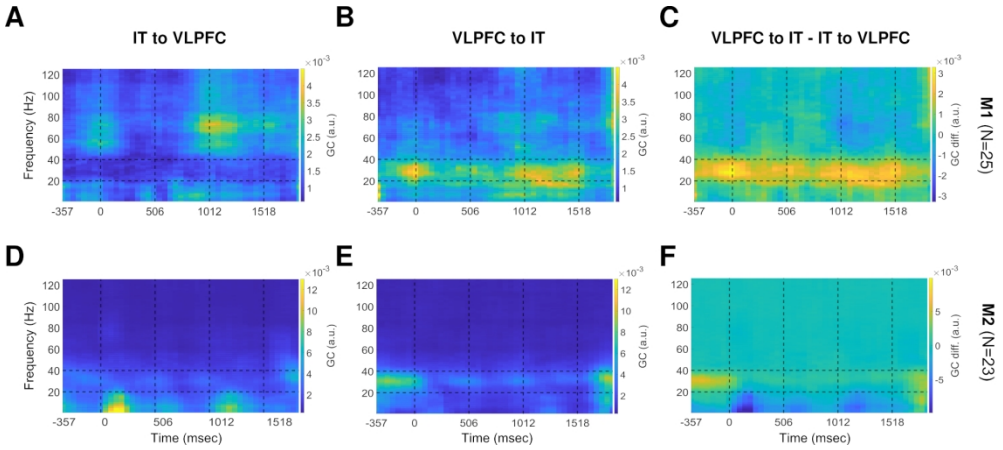

Figure 8

443x195mm (118 x 118 DPI)

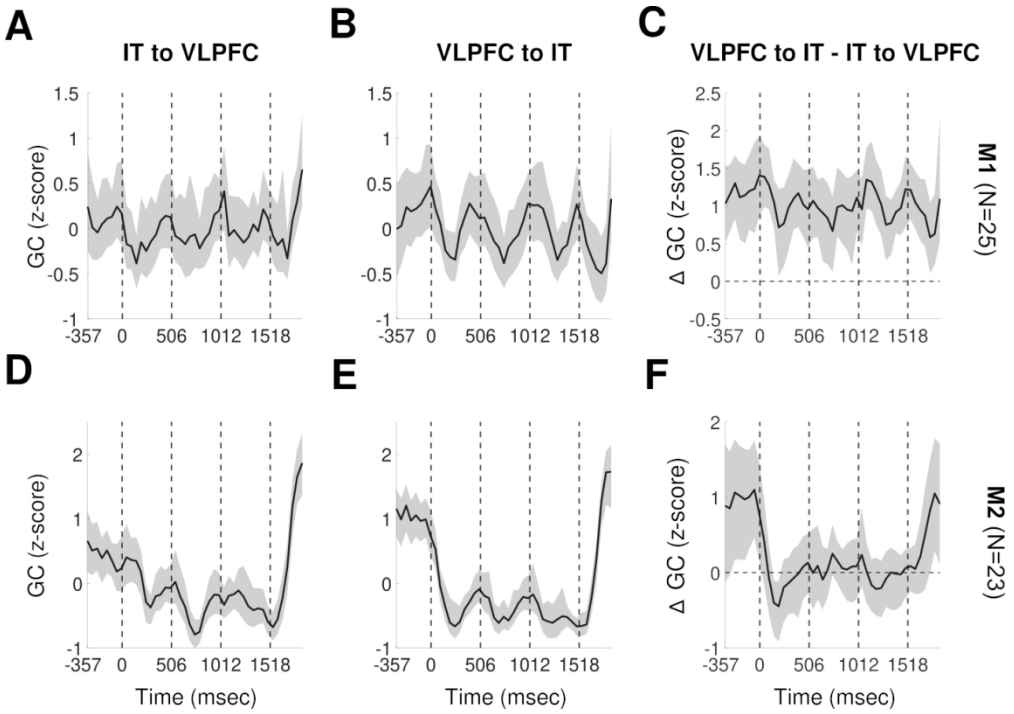

Figure 9

305x214mm (118 x 118 DPI)

Supplementary Material

Inferior temporal cortex leads prefrontal cortex in response to a violation of a learned sequence.

Hamideh Esmailpour, Rajani Raman and Rufin Vogels

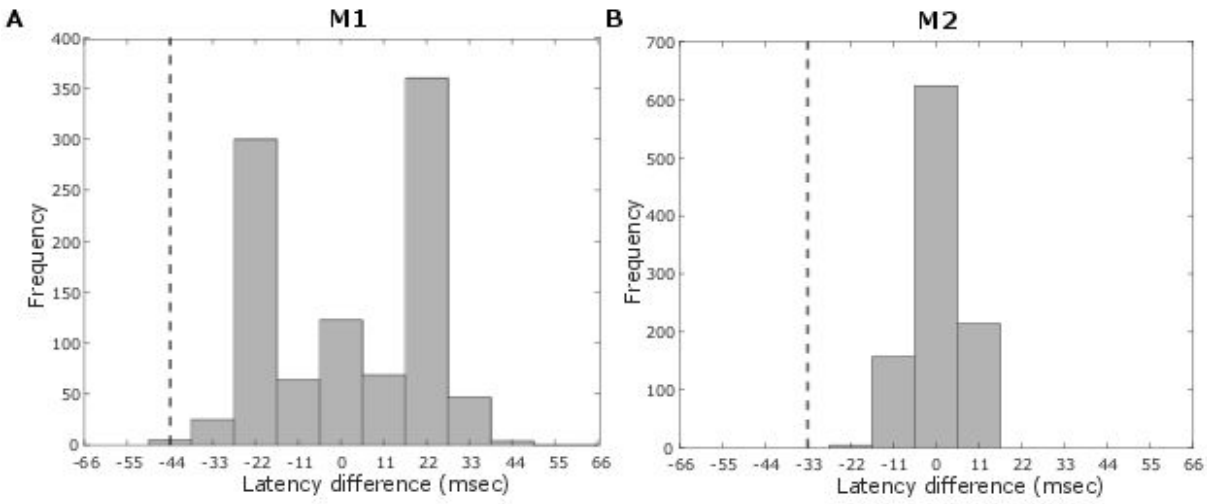

Figure S1: Null distribution of the permutation test of the difference in latency of the deviant response between IT and VLPFC (IT – VLPFC; see Methods). The dashed vertical line indicates the observed latency difference between the two areas. A. Data of M1. B. Data of M2.